Controllable optical mirror of cesium atoms with four-wave mixing*

Zhou Hai-Tao(周海涛)[a)b)], Wang Dan(王 丹)[a)], Guo Miao-Jun(郭苗军)[a)],
Gao Jiang-Rui(郜江瑞)[a)b)], and Zhang Jun-Xiang(张俊香)[a)†]

[a)] *The State Key Laboratory of Quantum Optics and Quantum Optics Devices, Institute of Opto-Electronics, Shanxi University, Taiyuan* 030006, *China*
[b)] *College of Physics and Electronics Engineering, Shanxi University, Taiyuan* 030006, *China*

(Received 1 April 2014; revised manuscript received 6 May 2014; published online 16 July 2014)

The controllable optical mirror is experimentally accomplished in a Λ-type three-level atomic system coupled with standing wave. It is shown that the reflection of probe light results from electromagnetically-induced-transparency-based four-wave mixing, therefore the reflection efficiency is highly dependent on the angle for phase matching condition between the probe and coupling fields. The measured reflection spectra show good agreement with dispersion compensation theory.

Keywords: optical mirror, four-wave mixing, phase mismatching, anomalous dispersion

PACS: 32.80.Qk, 42.50.Gy, 32.80.Wr, 42.50.Ct **DOI:** 10.1088/1674-1056/23/9/093204

1. Introduction

Electromagnetically induced transparency (EIT)[1] has received much attention in quantum optical information processing[2,3] as it is optically controllable and has been integrated on chips.[4] For a Λ-type three-level atomic system in hot atoms, the two-photon resonance for EIT needs to be Doppler-free, so that the traveling probe and coupling fields are co-propagating. When a standing-wave field formed by two counter-propagating fields was coupled to the Λ-type three-level system, other than transparent, a strong line-narrowed absorption of the probe light occurred,[5,6] which effect was explained as electromagnetically induced grating (EIG)[7–9] or four-wave mixing (FWM),[10,11] and even more exhibits the effect similar to that of optical photonic crystal, resulting from spatial periodic modulation of absorptions and group velocities in cold atoms,[12] which leads to the reverse probe light. In hot atoms, because of the Doppler shift, the atoms 'see' the counterpropagating coupling fields as bichromatic fields rather than a chromatic standing wave (SW), therefore an moving optical photonic crystal effect was established in atoms, and the function of all-optical optical diode was thus obtained.[13] Using the above atomic coherence process, the noise of interacting light was also discussed.[14–16]

In this paper, we use the spatially homogeneous Doppler-free FWM nonlinear atomic medium[12,17] to investigate the high reflection of the probe light. The comparison of Λ-type three-level system between two cases: $\omega_p > \omega_c$ and $\omega_p < \omega_c$ (ω_p is the angular frequency of the probe light and ω_c is that of the coupling field) is performed to support the dispersion compensation theory for phase matching condition. Furthermore, for the above two cases, the reflected efficiencies against the angle between the probe and coupling fields are experimentally demonstrated by changing the probe intensity and the Cs vapor temperature.

2. Experiment

The experiment is performed in a Λ-type three-level system of the D1 line of ^{133}Cs atom, which includes one excited state $|a\rangle$ ($6^2P_{1/2}, F' = 4$), and two ground states $|b\rangle$ ($6^2S_{1/2}, F = 4$) and $|c\rangle$ ($6^2S_{1/2}, F = 3$) (see Fig. 1(a)). The transition frequencies from $|a\rangle$ to $|b\rangle$ and $|c\rangle$ are ω_{ab} and ω_{ac}, respectively, and the frequency difference is $\delta = \omega_{ac} - \omega_{ab} = 2\pi \times 9.192$ GHz. The decay of the upper state to ground states is $\Gamma_a = 2\pi \times 4.6$ MHz. The arrangement of the experiment is shown in Fig. 1(b), the standing wave is created by two counter-propagating coupling beams, which come from an identical extended diode-laser and propagate from opposite directions through a 7.5-cm-long ^{133}Cs vapor cell with anti-reflection (AR) coated end windows. The vapor cell is mounted inside a three-layer μ-metal magnetic shield in order to reduce stray magnetic fields. Each of the coupling beams has a power of 20 mW with the parallel polarization. The probe light offered by another extended cavity diode laser has a power of 90 μW and its polarization is vertical. The values of e^{-2} full width of the probe and coupling beams are on the order of 0.59 mm and 0.64 mm, respectively. The crossing angle between co-propagating coupling and probe beams is denoted as θ. The transmission of the probe is detected by the photo detector PD1; photo detectors PD2 and PD3 are for detecting and estimating the polarization state of the reflected signal.

For Case A ($\omega_p > \omega_c$), the strong SW ($\omega_c = \omega_{cf} = \omega_{cb}$)

*Project supported by the National Natural Science Foundation of China (Grant Nos. 61308121 and 11274210) and the National Basic Research Program of China (Grant Nos. 2010CB923102 and 2011CB922203).

†Corresponding author. E-mail: junxiang@sxu.edu.cn

drives the transition from $|a\rangle$ to $|b\rangle$ with detuning $\Delta_{cf} = \Delta_{cb} = \Delta_c = \omega_c - \omega_{ab}$, and the weak probe field couples the transition between $|a\rangle$ and $|c\rangle$ with detuning $\Delta_p = \omega_p - \omega_{ac}$. Oppositely, for Case B, the transitions of the coupling field and probe field are exchanged (i.e., $\omega_p < \omega_c$, (see Fig. 1(a))).

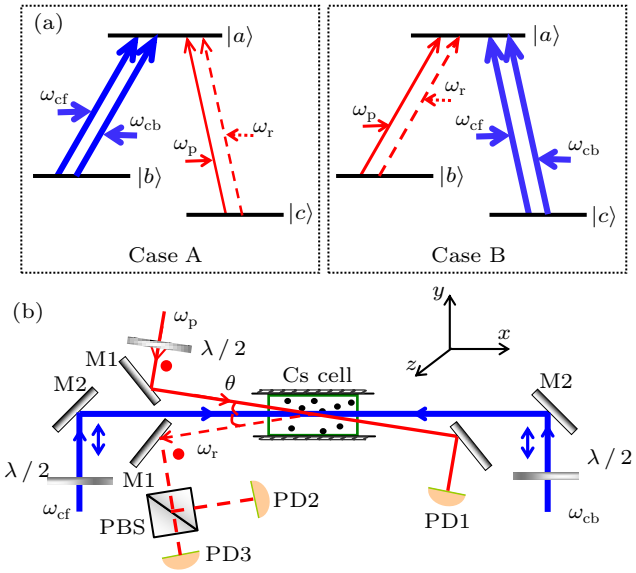

Fig. 1. (color online) (a) Λ-type three-level scheme. For Case A, $\omega_p > \omega_c$, and for Case B, $\omega_p < \omega_c$. (b) Experimental setup. $\lambda/2$ denotes the half wave plate, PBS the polarizing beam splitter, PD1–PD3 represent the photo detectors, M1 and M2 the mirrors, ω_p, ω_r, ω_{cf}, and ω_{cb} the frequencies of the probe, reflected, forward- and backward-propagating coupling light, respectively.

A reflected signal is generated (detected by PD2 in Fig. 1(b)) when the frequency of the coupling fields is locked at atomic resonant transition line ($\Delta_c = 0$), and meanwhile, the frequency of the probe is scanned. The reflection efficiency R (the ratio of the reflected signal power P_r to the input probe power P_p) versus the probe detuning Δ_p for different values of angle θ are plotted. For Case A (see Fig. 2(a)), the maximum reflection happens at $\theta = 0.42°$, and the power of reflected signal can reach more than 55% of the input probe power. There is a dip at $\Delta_p = 0$ ($\omega_p = \omega_{ac}$), which is due to the high absorption of hot atoms driven by two counter-propagating coupling fields. At an angle $\theta < 0.42°$ (or $\theta > 0.42°$), the angle-induced phase mismatch is positive (or negative), the peak appears at $\Delta_p > 0$ (or $\Delta_p < 0$), and the efficiency becomes small (see Fig. 2(c)). For Case B, the reflected peak always appears at $\Delta_p < 0$ (see Fig. 2(b)), and the efficiency decreases monotonically with the increase of angle θ (see Fig. 2(d)). This reflection effect of the probe field can be viewed as an optical mirror formed by the atom coupled with SW. Unlike the traditional glass mirror, however, it can be done only when the frequency of the probe is close to two-photon resonance (i.e., $\Delta_p = \Delta_c$), that is, the reflected line width of the atom–SW coupling mirror for the probe is narrower than that of the traditional glass mirror, which depend mainly on coating film, so that the reflected signal voids the influence of the Doppler background in the reflected direction, and the detection

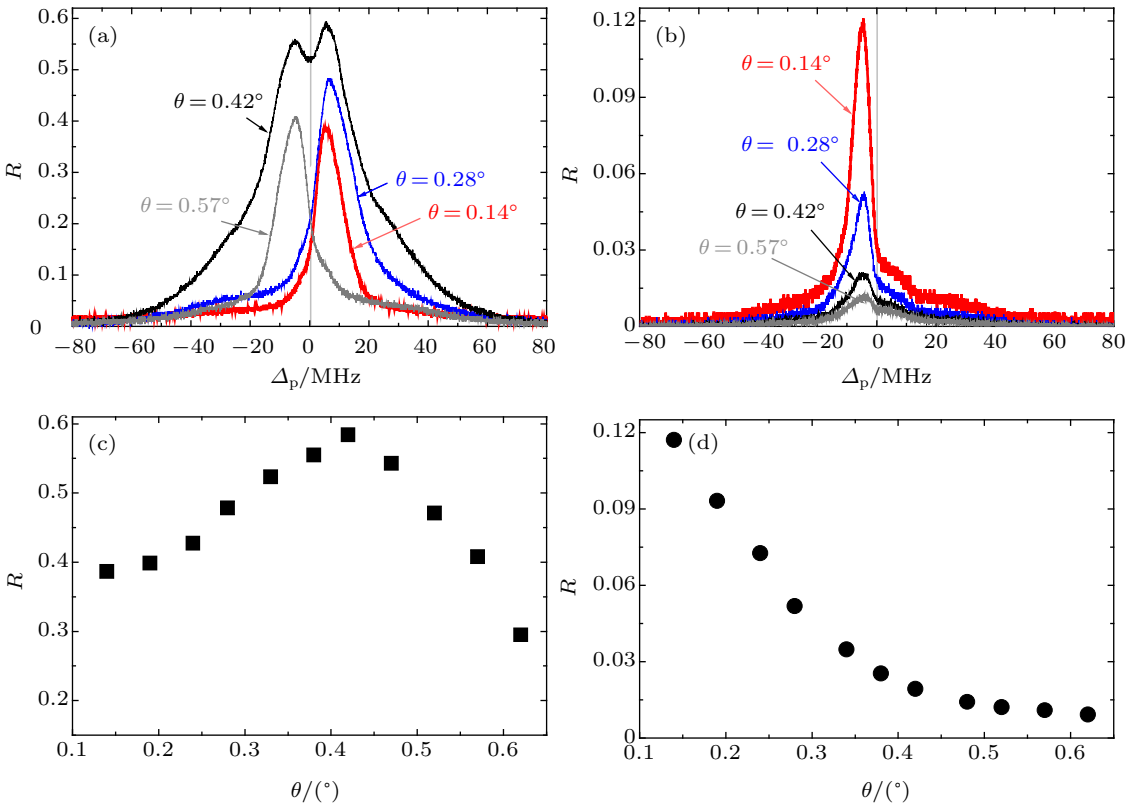

Fig. 2. (color online) (a) and (b) Curves of reflection signal versus probe detuning for different incident angles: $\theta = 0.14°$, $\theta = 0.28°$, $\theta = 0.42°$, $\theta = 0.57°$. (c) and (d) Tendency of the efficiency of reflection peaks versus angle θ. Panels (a) and (c) show the results for Case A; (b) and (d) the results for Case B. The experimental parameters are $P_p = 90$ μW, $P_{cf} = P_{cb} = 20$ mW, $T = 43$ °C, and $\Delta_c = 0$.

sensitivity to the reflection can be high.[18] On the other hand, the dispersion feature of the atoms on the probe light changes from the normal to the anomalous when the traveling wave (TW) coupling light is replaced by the SW coupling light, which can control the group velocity of the probe through in the cell.[19] The particular explanation about the angle dependence of positions of the reflection peak is theoretically analyzed in the next section.

3. Theoretical analysis

Now we turn to the theoretical analysis of this phenomenon. Naturally, the reflected FWM signal is due to the two Doppler-free two-photon resonant processes, which result in the coherent reflection from all the atoms in the vapor cell in the reflection direction. Consider a three-level system, in which the transition $|a\rangle \leftrightarrow |b\rangle$ (with the transition frequency being $\omega_{\rm ba}$) is coupled by a strong standing wave which is expressed as

$$\boldsymbol{E}_{\rm c}(\boldsymbol{r},t) = \left[E_{\rm cf}\,{\rm e}^{-{\rm i}(\omega_{\rm c}t-\boldsymbol{k}_{\rm cf}\cdot\boldsymbol{r})} + E_{\rm cb}\,{\rm e}^{-{\rm i}(\omega_{\rm c}t+\boldsymbol{k}_{\rm cb}\cdot\boldsymbol{r})}\right]\boldsymbol{y}/2 + {\rm c.c.},$$

where $E_{\rm cf}$ and $E_{\rm cb}$ are the amplitudes of the forward and backward coupling fields, respectively. A weak probe field $\boldsymbol{E}_{\rm p}(\boldsymbol{r},t) = E_{\rm p}\,{\rm e}^{-{\rm i}(\omega_{\rm p}t-\boldsymbol{k}_{\rm p}\cdot\boldsymbol{r})}\boldsymbol{z}/2 + {\rm c.c}$ induces the transition $|c\rangle \leftrightarrow |a\rangle$ (with transition frequency $\omega_{\rm ca}$). Because $E_{\rm p} \ll E_{\rm cf}$, $E_{\rm cb}$, the most atoms are populated at the level $|c\rangle$. Starting from this level, the atom absorbs one forward probe photon $\hbar\omega_{\rm p}$ and transits to level $|a\rangle$, then emits one forward coupling photon $\hbar\omega_{\rm c}$ and transits to level $|b\rangle$, then absorbs one backward photon $\hbar\omega_{\rm c}$ and transits to level $|a\rangle$, and finally generates one backward FWM photon $\hbar\omega_{\rm r}$ and transits to level $|c\rangle$. Therefore, the conservation of total energy leads to the generation of the reflected field accompanied by the enhancement of the co-propagating coupling field and the attenuations of the probe field and counter-propagating coupling field.

The efficiency of reflection induced by FWM is determined by many parameters, of which one is the phase matching condition $\Delta\boldsymbol{k} \equiv \boldsymbol{k}_{\rm p} - 2\boldsymbol{k}_{\rm c} - \boldsymbol{k}_{\rm r} = 0$, where $\boldsymbol{k}_{\rm c}$, $\boldsymbol{k}_{\rm p}$ and $\boldsymbol{k}_{\rm r}$ represent the wave vectors of the coupling, the probe and the reflected field, respectively, and $|\boldsymbol{k}_j| = n_j\omega_j/c$ $(j = {\rm c,p,r})$.

In Fig. 1(a), the value of $\Delta\boldsymbol{k}$ is

$$\begin{aligned}|\Delta\boldsymbol{k}| &= \Delta k_x = 2(n_{\rm p}\omega_{\rm p}\cos\theta - \omega_{\rm c})/c \\ &= 2(\omega_{\rm p}\cos\theta - \omega_{\rm c}) + {\rm Re}[\chi^{(1)}]\omega_{\rm p}\cos\theta]/c, \end{aligned} \quad (1)$$

$\chi^{(1)}$ is the linear susceptibility of the probe light, and its real part corresponds to the dispersion of the probe, and expressed as[9]

$$\chi^{(1)} = \int_{-\infty}^{+\infty} \frac{(-N|\mu_{\rm ac}|^2/\varepsilon_0\hbar)f(v)}{F_{\rm p} - F_1 - F_2}\,{\rm d}v, \quad (2)$$

where $F_{\rm p} = (\Delta_{\rm p} - \omega_{\rm p}v/c + {\rm i}\gamma_{\rm ac})$, $F_1 = \Omega_{\rm cf}(\Omega_{\rm cf}^* + \Omega_{\rm cb}^* Z_1)/[(\Delta_{\rm p} - \Delta_{\rm c}) + (\omega_{\rm c} - \omega_{\rm p})v/c + {\rm i}\gamma_{\rm cb}]$, and $F_2 = \Omega_{\rm cb}(\Omega_{\rm cb}^* + \Omega_{\rm cf}^* X_1)/[(\Delta_{\rm p} - \Delta_{\rm c}) - (\omega_{\rm p} + \omega_{\rm c})v/c + {\rm i}\gamma_{\rm cb}]$, with $\Omega_{\rm cf}$ and $\Omega_{\rm cb}$ being the Rabi frequencies of the forward and backward coupling fields, respectively. Considering the atoms in vapor cell, we need to perform the integration over velocity distribution $f(v) = (m/2\pi k_{\rm B}T)^{1/2}\exp(-mv^2/2k_{\rm B}T)$, and make the average over all Doppler detuning by replacing the detuning $\Delta_{\rm cf} \to \Delta_{\rm c} - (\omega_{\rm c}v/c)$, $\Delta_{\rm p} \to \Delta_{\rm p} - (\omega_{\rm p}v/c)$, and $\Delta_{\rm cb} \to \Delta_{\rm c} + (\omega_{\rm c}v/c)$. Figure 3(c) shows the theoretical calculations for the real part of $\chi^{(1)}$ in Eq. (2). We can see that the dispersion is anomalous (solid line in Fig. 3(c)) when $\Omega_{\rm cf} = \Omega_{\rm cb}$. For only forward coupling field with $\Omega_{\rm cb} = 0$, the dispersion is normal (see dashed line in Fig. 3(c)).

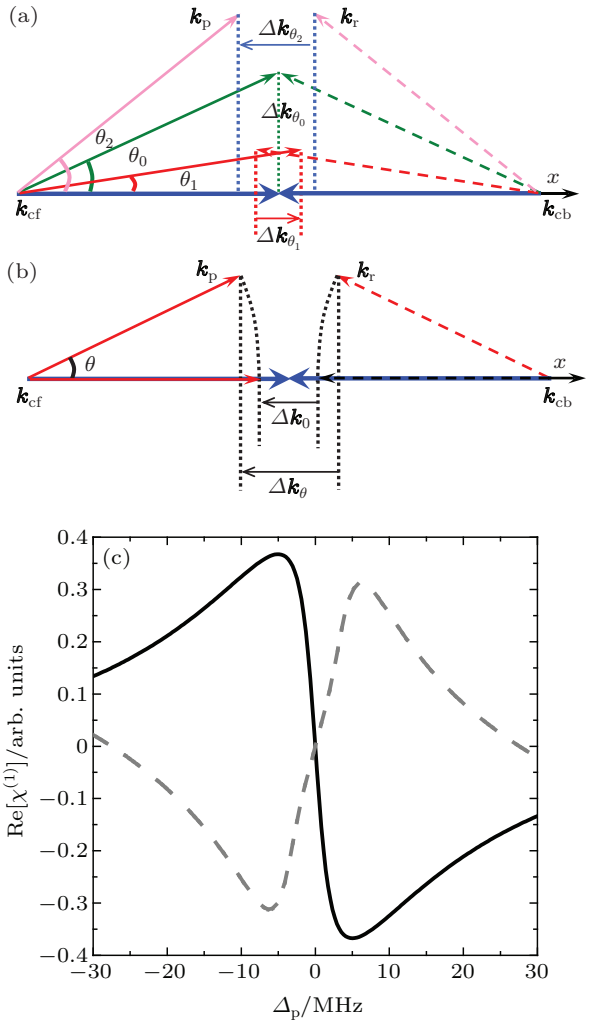

Fig. 3. (color online) The scheme of phase mismatching in the two- and one- photon resonance ($\Delta_{\rm p} = \Delta_{\rm c} = 0$) for Case A: $\omega_{\rm p} > \omega_{\rm c}$ (a) and Case B: $\omega_{\rm p} < \omega_{\rm c}$ (b). (c) Curves of the real part of linear susceptibility $\chi^{(1)}$ versus the probe detuning.

In order to investigate the effect of probe dispersion on the FWM efficiency, we separate the wave vector mismatch into two parts, $\Delta k_x = \Delta k_\theta + \Delta k_{\rm d}$, on the right-hand side of the above expression the first term $\Delta k_\theta = 2(\omega_{\rm p}\cos\theta - \omega_{\rm c})/c$ is the angle-induced wave vector mismatch in free vacuum, and the second term $\Delta k_{\rm d} = (\omega_{\rm p}/c){\rm Re}[\chi^{(1)}]$ is the dispersion-induced wave vector mismatch. For Case A, the phase match-

ing condition $\Delta k_x = 0$ occurs at a value $\theta_0 = 0.42°$ with one- and two-photon resonances ($\Delta_p = \Delta_c = 0$), so that the efficiency is the highest. We should emphasize that the role of the phase compensation Δk_d due to the anomalous dispersion occurs around θ_0. From Fig. 3(a) it follows that for $\theta_1 < 0.42°$ and $\Delta k_{\theta 1} > 0$, the phase matching condition can be satisfied only if $\Delta k_d < 0$, which happens at $\Delta_p > 0$ because of the anomalous dispersion of $\mathrm{Re}[\chi^{(1)}]$, so that the peak appears at $\Delta_p > 0$ (see Fig. 2(a)). On the other hand, for $\theta_2 > 0.42°$, the phase compensation induced by the anomalous dispersion leads to the peak appearing at $\Delta_p < 0$. Similarly, for Case B ($\omega_p < \omega_c$), because the phase is always mismathing $\Delta k_\theta < 0$, no matter what θ is (see Fig. 3(b)), only the $\mathrm{Re}[\chi^{(1)}] > 0$ can compensate for the phase mismatching, so the peak appears at $\Delta_p < 0$ (see Fig. 2(b)).

The efficiency of FWM is also related to real part of the third order nonlinear susceptibilitie $\chi^{(3)}$,[20] which can be obtained from the nonlinear polarization $P(\omega_p - \omega_{cf} + \omega_{cb}) = 6\varepsilon_0\chi^{(3)}E_pE_{cf}^*E_{cb}$. The detailed theoretical analysis can be found in Ref. [9]. Now we numarically caculate the values of reflection efficiency R as a function of probe detuning for Case A and Case B (see Fig. 4). The theoretical calculations are well consistent with the experimental results.

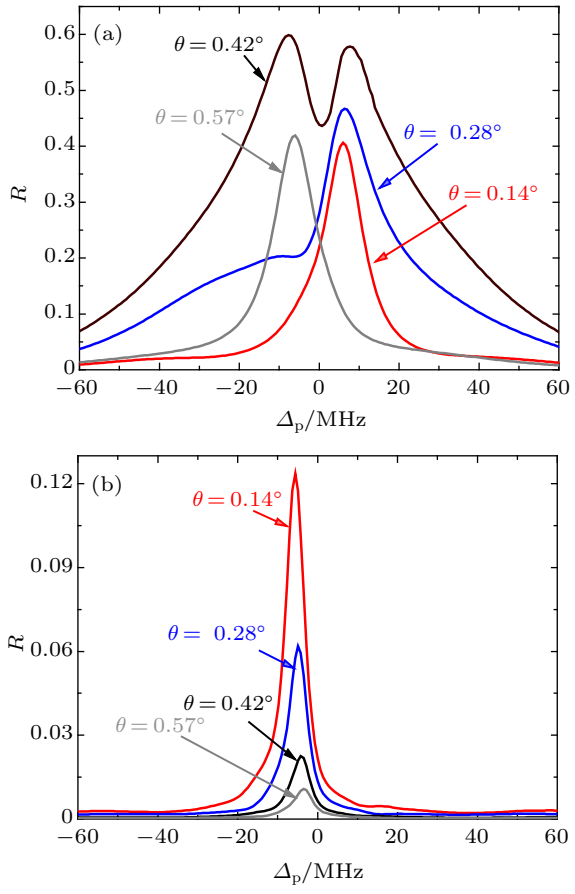

Fig. 4. (color online) Numerical calculations for reflected signal versus the probe detuning at different angles for Case A (a) and Case B (b): $\theta = 0.14°$, $0.28°$, $0.42°$, and $0.57°$.

4. Dependences of reflected efficiency on other parameters

Apart from the angle for phase matching condition, the reflected efficiency is also dependent on other parameters, such as the intensity of the probe. The dependences of the reflection efficiency on incident probe intensity for Cases A and B are different from each other (see Fig. 5). When $\theta = 0.42°$ in Case A, as $\Delta k_x = 0$ at $\Delta_p = \Delta_c = 0$, the phase is matched. It is shown that the reflection efficiency R increases from 50% to 60% as P_p increases from 10 μW to 100 μW, and then reaches a saturation value and is nearly unchanged as P_p increases to 1 mW (see black triangles in Fig. 5(a)). Unlikely, however, at the phase mismatching angle, e.g., $\theta = 0.14°$ (see gray squares), R decreases from 43% to 15% as P_p increases from 10 μW to 1 mW. This effect can be understood from the phase compensation: at the phase mismatching angle, $\Delta k_x \neq 0$, the FWM is promoted by dispersion compensation Δk_d, which is mainly affected by the first order susceptibility $\chi^{(1)}$. However, increasing the probe power breaks the population of the ground state, which modifies the $\chi^{(1)}$, so it diminishes the dispersion-induced phase compensation. The same variation appears for Case B (see Fig. 5(b)), no matter what θ is, R decreases with increasing P_p.

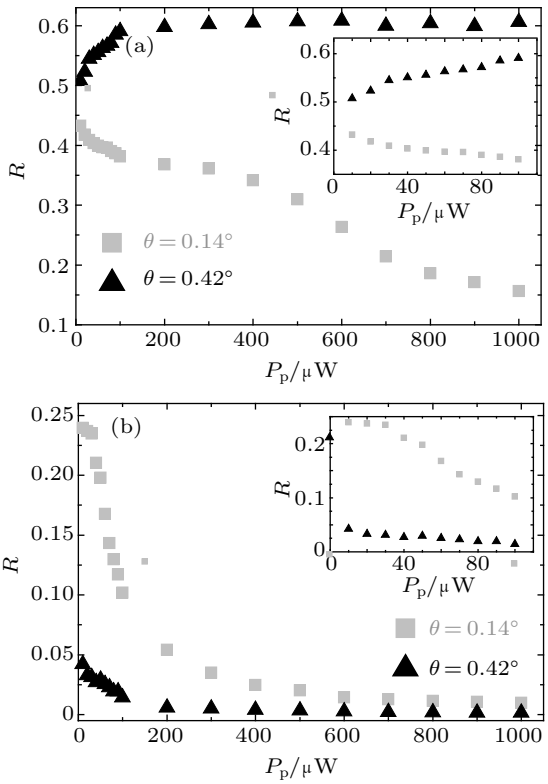

Fig. 5. (color online) Efficiencies of reflection peak versus the power of probe for different angles: $\theta = 0.14°$ (gray squares) and $0.42°$ (black triangles) for Case A ($\omega_p > \omega_c$) (a) and Case B (b), at $\omega_p < \omega_c$. The other experimental parameters are the same as those in Fig. 2.

When the phase matching condition is satisfied for Case A at $\theta = 0.42°$, the reflection efficiency first increases with

the increase of probe power, and then keeps the value of 60% when the probe power is higher than 100 μW, in which range of power, the mirror property with 60% reflection is created. However the reflection is reduced with the increase of the input probe power when the phase matching condition is not satisfied ($\Delta k \neq 0$) for Case A and for Case B. The width of reflection spectrum is also dependent on power, and the underlying mechanism is complicated: one of effects is due to the dispersion compensation. Figure 6 shows the reflected spectra in different probe powers for Case B at $\theta = 014°$. When $P_p = 50$ μW, the full width at half maximum (FWHM) of the reflected signal is about 8 MHz (see line 1 in Fig. 6), and when P_p increases to 500 μW, the FWHM rises up to 36 MHz (see line 5 in Fig. 6). The dip in atomic resonance center is due to the high absorption of the hot atoms driven by two counter-propagating coupling fields.[10] The complex reflection of FWM process may be useful for further studying the nonlinear wave-fixing or slow and fast light effect in small two-photon detuning.

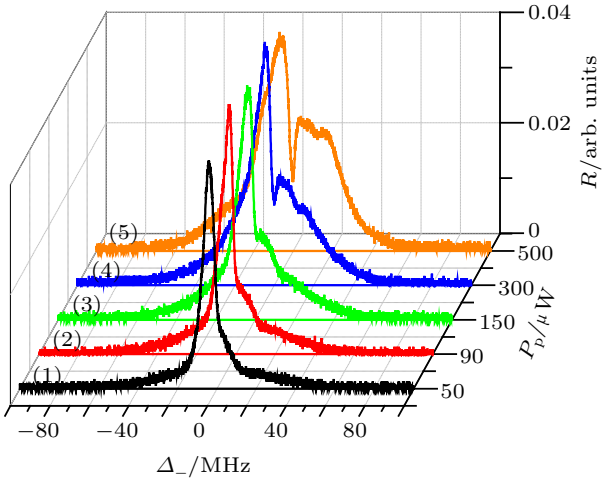

Fig. 6. (color online) Reflection spectra versus the probe detuning at different powers of the probe light for Case B. $\theta = 014°$, and the other experimental parameters are the same as those in Fig. 2.

On the other hand, the FWM efficiency can also be controlled by changing the temperature of the vapor cell as shown in Fig. 7. It is seen that the reflection efficiency increases with the increase of the temperature, and reaches a saturation value at $T = 63$ °C for Case A (at $T = 87$ °C for Case B) at any angle θ. The reflection reaches as high as 60% at $\theta = 0.42°$ for Case A (black squares in Fig. 7(a)), and as high as 44% at $\theta = 0.14°$ for Case B (circles in Fig. 7(b)). As the higher vapor temperature means the larger atomic number density N, here N is proportional to the first and the third nonlinear susceptibility $\chi^{(1)}$ and $\chi^{(3)}$, whose real parts determine the degree of dispersion compensation and the nonlinear efficiency, respectively. For higher temperature, however, the rising of temperature may induce other nonlinear effects,[21,22] which will lead to the reduction of reflection efficiency.

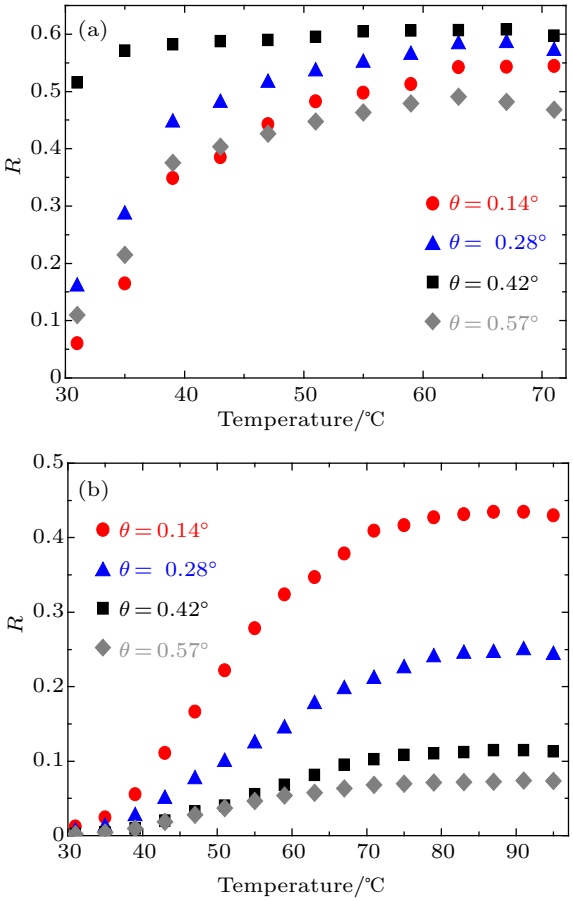

Fig. 7. (color online) Efficiencies of reflection peak versus temperature of Cs vapor at $\theta = 0.14°$, 0.28°, 0.42°, and 0.57° for Case A (a) and Case B (b). The other experimental parameters are the same as that in Fig. 2.

5. Conclusion

In this paper, we experimentally and theoretically investigate the high-efficiency FWM in the Cs vapor under two counter-propagating coupling fields. It can be used as an optical reflection mirror and controlled by changing the angle between the probe and the coupling light, the probe intensity and the temperature of the atom vapor. Especially, the controllable property of the reflection signal can be accomplished by changing the angle based on the phase compensation theory of anomalous dispersion. This study may provide the guidance for studying the multi-channel quantum logic gate operation and quantum information processing.

References

[1] Boller K J, Imamoğlu A and Harris S E 1991 *Phys. Rev. Lett.* **66** 2593
[2] Eisaman M D, Andre A, Massou M, Fleischhauer M, Zibrov A S and Lukin M D 2005 *Nature* **438** 837
[3] Fleischhauer M, Imamoğlu A and Marangos J P 2005 *Rev. Mod. Phys.* **77** 633
[4] Wu B, Hulbert J F, Lunt E J, Hurd K, Hawkins A R and Schmidt H 2010 *Nat. Photonics* **4** 776
[5] Feldman B J and Feld M S 1972 *Phys. Rev. A* **5** 899
[6] Affolderbach C, Knappe S, Wynands R, Taichenachev A V and Yudin V L 2002 *Phys. Rev. A* **65** 043810

[7] Cardoso G C and Tabosa J W R 2002 *Phys. Rev. A* **65** 033803
[8] Brown A W and Xiao M 2005 *Opt. Lett.* **30** 699
[9] Su X M, Zhuo Z C, Wang L J and Gao J Y 2002 *Chin. Phys.* **11** 35
[10] Zhang J X, Zhou H T, Wang D W and Zhu S Y 2011 *Phys. Rev. A* **83** 053841
[11] Zhang Y L, Jiang L, Sun Z R, Ding L E and Wang Z G 2003 *Chin. Phys.* **12** 174
[12] Artoni M and Rocca G C L 2006 *Phys. Rev. Lett.* **96** 073905
[13] Wang D W, Zhou H T, Guo M J, Zhang J X, Evers J and Zhu S Y 2013 *Phys. Rev. Lett.* **110** 093901
[14] Zhang Y P, Wu H C, Wang P F and Li C S 2000 *Chin. Phys.* **9** 599
[15] Li Z H, Li Y, Dou Y F and Zhang J X 2012 *Chin. Phys. B* **21** 034204
[16] Li Z H, Li Y, Dou Y F, Gao J R and Zhang J X 2012 *Chin. Phys. Lett.* **29** 014202
[17] Kuang S Q, Wan R G, Du P, Jiang Y and Gao J Y 2008 *Opt. Express* **16** 15455
[18] Mitsunaga M and Imoto N 1999 *Phys. Rev. A* **59** 4773
[19] Bae I H and Moon H S 2011 *Phys. Rev. A* **83** 053806
[20] Zhou H T, Wang D W, Wang D, Zhang J X and Zhu S Y 2011 *Phys. Rev. A* **84** 053835
[21] Guo M J, Zhou H T, Wang D, Gao J R, Zhang J X and Zhu S Y 2014 *Phys. Rev. A* **89** 033813
[22] Zhang X H, Hu X M, Kong L F and Zhang X 2010 *Chin. Phys. B* **27** 094208